



Metal-organic framework derived Cu/ZnO catalysts for continuous hydrogenolysis of glycerol



Liping Zheng^a, Xuewen Li^a, Weichen Du^a, Danwei Shi^a, Wensheng Ning^b, Xiuyang Lu^a, Zhaoyin Hou^{a,*}

^a Key Laboratory of Biomass Chemical Engineering of Ministry of Education, Department of Chemistry, Zhejiang University, Hangzhou 310028, China

^b State Key Laboratory Breeding Base of Green Chemistry-Synthesis Technology, Zhejiang University of Technology, Hangzhou 310032, China

ARTICLE INFO

Article history:

Received 25 July 2016

Received in revised form 5 October 2016

Accepted 8 October 2016

Available online 11 October 2016

Keywords:

Cu/ZnO
HKUST-1
Glycerol
Hydrogenolysis
1,2-propanediol

ABSTRACT

Cu/ZnO catalysts are widely used in industrial production, environmental protection and biorefinery, finding a new and efficient method for the controlled synthesis of Cu/ZnO hybrid is of great importance. In this work, a novel Cu/ZnO catalyst with nano sized ZnO particles dotted on Cu was synthesized via the calcination and reduction of Cu(Zn)-HKUST-1 precursor. The transformation process from Cu(Zn)-HKUST-1 to Cu/ZnO was characterized by TG-DSC, XRD, XPS and TEM. And the performance of final Cu/ZnO catalysts for continuous hydrogenolysis of glycerol was tested in a fixed-bed reactor. It was found that Cu_{1.1}/ZnO catalyst derived from Cu_{1.1}Zn_{1.9}(BTC)₂·9.4(H₂O) was more active and stable than Cu/ZnO that prepared via solvent-free grinding and co-precipitation. Characterizations results also inferred that the interface between Cu and ZnO played a crucial role on its catalytic performance, and ZnO dotted Cu was more stable than ZnO plate supported Cu particles.

© 2016 Elsevier B.V. All rights reserved.

1. Introduction

Cu/ZnO catalysts are of great importance in industrial methanol synthesis [1,2], low-temperature water–gas shift reaction [3], and selective catalytic reduction of NO_x [4]. At the same time, Cu/ZnO is also a promising candidate for the steam reforming of alcohol to hydrogen production [5–9] and for biomass conversion to sustainable chemicals [10–12]. Among of which, its application in the selective hydrogenolysis of glycerol, an oversupplied by-product during the manufacture of biodiesel, has attracted much attentions in the past decade [12–22]. The performance of Cu/ZnO catalysts in the hydrogenolysis of glycerol was well summarized by Nakagawa [23] and Wang [24].

It is of great importance to find a new and efficient strategy for the controlled synthesis of Cu/ZnO catalyst [1–3]. A lot of approaches were reported for the synthesis of highly active and stable Cu/ZnO catalysts [12,25,26], and the recent achievements were disclosed by Kuld [2], Kondrat [3] and van den Berg [27]. In these works, Kondrat et al. pointed out that the most often preparation method, co-precipitation, using sodium carbonate as the carbonate

source would introduce sodium ions – a potential catalyst poison [3].

At the same time, it has been popularly accepted that the activity of Cu-based catalysts depended mainly on the dispersion of Cu, and small sized Cu particles were more active than large ones [14,28]. For example, surface Cu species were identified as the primary active sites for hydrogenolysis of glycerol, and the yield of 1,2-propanediol (1,2-PDO) increased with the increasing surface area of Cu [23,24,29–32]. However, the latest achievements disclosed that the interfacial area between Cu and ZnO played a crucial role for the activity and stability of Cu/ZnO catalyst in methanol synthesis [2,26,33]. Unfortunately, the role of interface between Cu and ZnO in hydrogenolysis of glycerol was seldom reported.

Metal-organic frameworks (MOFs) are coordination networks with organic ligands containing potential voids [34]. The chemical composition and the shape of building units of MOFs can be multiply varied within a particular structure already exist [35]. These characteristics allow the interior of MOFs to be chemically altered for application in lithium-ion battery [36], photocatalysis [37,38], hydrogenation of nitroarenes [39], gas sorption [40], and Fischer-Tropsch Synthesis [41]. Among of which, [Cu₃(BTC)₂·9.4(H₂O), BTC=benzene-1,3,5-tricarboxylic acid], also known as HKUST-1, contains large cavities [42], could be synthesized quickly without the participation of sodium ion [43].

* Corresponding author.

E-mail address: zyhou@zju.edu.cn (Z. Hou).

In this work, we want to report our effort in the synthesis of Cu/ZnO catalysts via controlled calcination and reduction of $\text{Cu}_x\text{Zn}_{3-x}(\text{BTC})_2 \cdot 9.4(\text{H}_2\text{O})$. The transformation process from $\text{Cu}_x\text{Zn}_{3-x}(\text{BTC})_2 \cdot 9.4(\text{H}_2\text{O})$ to Cu/ZnO catalyst was characterized by thermogravimetry-differential scanning calorimetry (TG-DSC), in-situ X-ray diffraction, X-ray photoelectron spectra (XPS) and transmission electron microscopy (TEM). The performance of final Cu/ZnO for the continuous hydrogenolysis of glycerol was carried out in fixed-bed reactor as a model reaction, and special attentions were paid on the interfacial area between Cu and ZnO.

2. Experiments

2.1. Synthesis of Cu(Zn)-HKUST-1

At first, ZnO powder (36 mmol) was dispersed in 80 mL deionized water, treated with sonication for 10 min to form a nano-slurry (denoted as solution A). $\text{Cu}(\text{NO}_3)_2 \cdot 3\text{H}_2\text{O}$ (containing 18, 36, 72 mmol Cu^{2+}) was dissolved in 80 mL deionized water (denoted as solution B). Benzene-1,3,5-tricarboxylic acid (H_3BTC , 36, 48, 72 mmol) was dissolved in 260 mL ethanol (denoted as solution C). And then, solution A was mixed with 160 mL *N,N*-Dimethylformamide (DMF), to which, solution B and C were added consecutively under vigorously stirring. One minute later, the solid product was immediately filtered off with a polypropylene membrane filter (0.45 μm pore size) and washed with ethanol for 3 times. The as-synthesized $\text{Cu}_x\text{Zn}_{3-x}$ -HKUST-1 product was further dried in vacuum at 120 °C for 6 h [44].

Before catalytic reaction, $\text{Cu}_x\text{Zn}_{3-x}$ -HKUST-1 precursors were heated slowly (2 °C/min) to 400 °C and calcined at 400 °C in a flow of air for 4 h. The calcined products were identified as $\text{Cu}_x\text{Zn}_{3-x}\text{O}_3$. Then the calcined $\text{Cu}_x\text{Zn}_{3-x}\text{O}_3$ was further reduced in hydrogen flow (80 mL/min) at 350 °C for 1 h before the hydrogenolysis reaction, and these reduced catalysts were identified as Cu/ZnO.

Cu-ZnO catalysts were also prepared according to the method of solvent-free grinding (denoted as Cu-ZnO-SF) [45] and co-precipitation (denoted as Cu-ZnO-CP) [3], and used as references. After reduction, they were marked as Cu/ZnO-SF and Cu/ZnO-CP, respectively. Their preparation procedures were described in detail in the electronic Supplementary materials. The composition of above prepared Cu-ZnO catalysts were detected on inductively coupled plasma-atomic emission spectroscopy (ICP, Plasma-Spec-II spectrometer), and the content of Cu and Zn were summarized in Table 1.

2.2. Characterization

N_2 adsorption was measured at its normal boiling point using an ASAP 2010 analyzer (Micromeritics) after pretreated at 250 °C for 4 h in vacuum. Specific surface area was calculated using Brunner-Emmet-Teller (BET) method in the range of $\text{P}/\text{P}_0 = 0.0-0.06$ (for MOFs) or 0.05-0.30 (for other samples), and pore size distribu-

tions were calculated using the Density functional theory (DFT) (for MOFs) or Barrett-Joyner-Halenda (BJH) method (for other samples). Power X-ray diffraction (XRD) patterns of fresh and calcined $\text{Cu}_x\text{Zn}_{3-x}$ -HKUST-1 were detected at room temperature on a Rigaku D/WAX-2500 diffractometer using $\text{Cu K}\alpha$ radiation ($\lambda = 1.5406 \text{ \AA}$) with a 20 step of 0.02°, and 5°/min from 5 to 80°. In-situ XRD analysis of reduced $\text{Cu}_{1.1}\text{Zn}_{1.9}\text{O}_3$ at different temperature in 5% H_2/Ar flow (30 mL/min) was carried out on the same system connected to an Anton-Paar high-temperature XRD assembly in which sample was mounted in a high-temperature cell, heated at 10 °C/min, and stabilized for 5 min at each temperature before measurements. X-ray photoelectron spectroscopy (XPS) measurements were performed on a KratosAxis Ultra DLD system with a base pressure of 10^{-9} Torr. TG-DSC was carried out on a Netzsch STA 409 thermobalance. Analysis was done from 25 to 450 °C at a heating rate of 10 °C/min in air flow (30 mL/min). Transmission electron microscope (TEM) images were obtained using an accelerating voltage of 200 kV (JEOL-2020F). The sample was suspended in ethanol with an ultrasonic dispersion for 0.5 h. Drops of the suspension were deposited on nickel grid coated with amorphous carbon film. Scanning electron microscope (SEM) images were detected on Leo Evo Series SEM (VP 1430, Germany). Samples were coated with platinum using sputter coating to avoid charging. Analysis was carried out at an accelerating voltage of 5 kV. Energy dispersive spectroscopy (EDS) analysis was carried out at an accelerating voltage of 15 kV.

Temperature-programmed reduction (H_2 -TPR) of calcined $\text{Cu}_x\text{Zn}_{3-x}\text{O}_3$ was performed in the following procedures: samples (50 mg) were pretreated at 400 °C for 1 h in Ar flow (30 mL/min) and cooled to room temperature. A reduction gas (10% H_2/N_2 mixture, 30 mL/min) was shifted and the reactor was heated to 400 °C at a ramp of 10 °C/min. Effluent gas was dried by powder KOH and the consumption of hydrogen was recorded by thermal conductivity detector (TCD). The amount of reduced Cu in these samples was calibrated with pure CuO (AR, Sinopharm Chemical Reagent Co., Ltd, China) of known amount. The number of surface metallic Cu was determined by N_2O oxidation and followed H_2 titration using the procedure described by Van Der Grift et al. [46]. H_2 activation on reduced catalysts was checked via H_2 temperature-programmed desorption (H_2 -TPD). The sample was first reduced at 350 °C in H_2 flow (30 mL/min) for 1 h, purged with purified Ar. Then the reactor was cooled to 50 °C in Ar, exposed to 10% H_2/N_2 mixture for 30 min, and purged with Ar for 5 h at 50 °C in order to eliminate the physically adsorbed H_2 . After that, the reactor was heated to 400 °C at a ramp of 10 °C/min in Ar flow (30 mL/min), and hydrogen in effluent was recorded by a TCD detector.

2.3. Catalytic reaction

Hydrogenolysis of glycerol was carried out in a vertical fixed-bed reactor with a back pressure regulator to control the system pressure. The reactor was a stainless steel tube with an internal diameter of 6 mm and a length of 540 mm. In a typical run, 0.1-0.5 g catalyst (40–60 mesh) was loaded in the constant temperature zone of the reactor, with quartz sand packed in both ends. Before reaction, catalyst was in situ reduced in pure H_2 flow (80 mL/min) at 350 °C for 1 h. After reduction, the reactor was cooled to reaction temperature and pressured to 2.0 MPa. An aqueous solution of glycerol (20 wt% glycerol) was continuously fed into the reactor with a flow rate of 0.02 mL/min. The reaction products were cooled in a condenser (remained at -5 °C) and collected in a gas-liquid separator. Gas phase effluent was diverted into a gas loop and analyzed using a gas chromatograph (HP5890, series II, equipped with a TDX-01 (4 mm × 2 m) column and a TCD detector). Liquid samples were collected at regular intervals of time and analyzed using a gas chromatograph (Shimadzu, 14B) equipped with a 30-

Table 1
Content of Cu and Zn in Cu/ZnO catalysts.

Catalyst	Bulk composition ^a after calcination			Surface composition ^b after reduction		
	Cu	Zn	Zn/Cu	Cu	Zn	Zn/Cu
$\text{Cu}_{2.8}\text{Zn}_{0.2}\text{O}_3$	47.1	3.0	0.06	84.0	8.0	0.10
$\text{Cu}_{1.7}\text{Zn}_{1.3}\text{O}_3$	28.6	21.4	0.75	37.0	31.5	0.85
$\text{Cu}_{1.1}\text{Zn}_{1.9}\text{O}_3$	19.0	31.0	1.63	14.0	43.0	3.07
Cu-ZnO-SF	19.1	30.9	1.62	11.5	44.2	3.84
Cu-ZnO-CP	16.7	33.4	2.00	32.4	33.8	1.04

^a Calculated from the results of ICP.

^b Calculated from survey scan results of XPS.

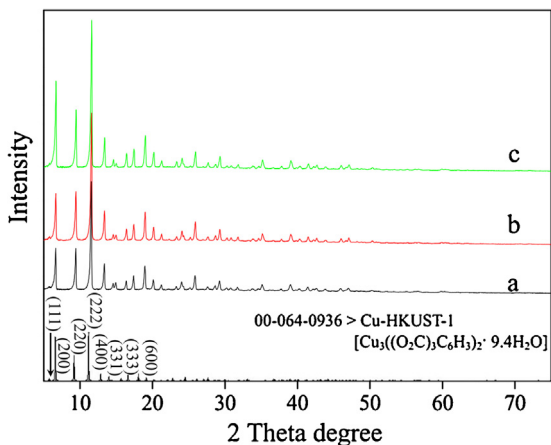


Fig. 1. XRD patterns of fresh Cu_{1.1}Zn_{1.9}-HKUST-1 (a), Cu_{1.7}Zn_{1.3}-HKUST-1 (b) and Cu_{2.8}Zn_{0.2}-HKUST-1 (c).

m capillary column (DB-WAX 52 CB, USA) and flame ionization detector. All products detected in the liquid were verified by a gas chromatography-mass spectrometry system (GC-MS, Agilent 6890) and quantified via an external calibration method. Each analysis was carried out after a steady operation for 2 h, and the product selectivity was calculated on carbon basis. The mass balances in liquid phase were higher than 97% in all experiments.

3. Results and discussion

3.1. The structure Cu_xZn_{3-x}-HKUST-1 precursor

XRD analysis confirmed that the primary structure of original Cu-HKUST-1 (JCPDS, 00-064-0936) remained stable when Cu was partially substituted by Zn (see Fig. 1). Very similar peak profiles and intensities were observed for all synthesized samples (with different Zn/Cu mole ratio), which indicated the homogenous substitution of Zn in Cu-HKUST-1, without distortion of HKUST-1 framework. The calculated cell parameters of these samples were similar as that of Cu-HKUST-1 (see Table 2) [42,47]. The synthesized Cu_{1.1}Zn_{1.9}-HKUST-1 crystal with an octahedral outline was also observed clearly in its SEM images (see Fig. S1).

N₂ sorption isotherms of all fresh HKUST-1s were type I model with the rapid rise of N₂ uptake at 0–0.02 of P/P₀ (Fig. 2A), which was the characteristic of microporous material. The calculated BET surface areas of Cu_{1.1}Zn_{1.9}-HKUST-1, Cu_{1.7}Zn_{1.3}-HKUST-1, Cu_{2.8}Zn_{0.2}-HKUST-1 were 1609, 1748 and 1648 m²/g, respectively

Table 2
Lattice parameters and surface area of synthesized Cu_xZn_{3-x}-HKUST-1.

Catalyst	$a=b=c$ (nm) ^a	S_{BET} (m ² /g) ^b
Cu _{1.1} Zn _{1.9} -HKUST-1	2.6519	1609
Cu _{1.7} Zn _{1.3} -HKUST-1	2.6427	1748
Cu _{2.8} Zn _{0.2} -HKUST-1	2.6336	1648
Cu-HKUST- ^c	2.6343	–

^a Calculated from results of XRD using the peak of HKUST-1 (200), Bragg Equation.

^b Calculated by BJH method from their adsorption isotherms.

^c Data that reported in reference [S.S.-Y. Chui, S.M.-F. Lo, J.P.H. Charmant, A.G. Orpen, I.D. Williams, Science 283 (42) 1148–1150].

(Table 2). The higher surface area of Cu_{1.7}Zn_{1.3}-HKUST-1 could be attributed to the phenomenon that the density of HKUST-1 framework decreased when Cu was partially substituted by Zn [48]. However, excessive Zn contents in Cu_{1.1}Zn_{1.9}-HKUST-1 decreased its surface area. All synthesized Cu_xZn_{3-x}-HKUST-1 had a well-distributed microporous channels at 0.87 nm, corresponding to the primary pore of HKUST-1 (see Fig. 3) [42]. And it was interesting to note that tiny amount of mesoporous channels (with the diameter of 4.10 nm) also appeared in Cu_{1.7}Zn_{1.3}-HKUST-1 and Cu_{2.8}Zn_{0.2}-HKUST-1 (see the insert in Fig. 2B).

3.2. Synthesis of Cu/ZnO catalysts from Cu(Zn)-HKUST-1

TG-DSC analysis showed that there were two major weight losses during the calcination of Cu_{1.1}Zn_{1.9}-HKUST-1. The first weight loss at 25–305 °C with a small endothermic peak was attributed to the volatilization of water, and the second loss at 305–354 °C with a strong exothermic signal was owing to the combustion of (BTC)³⁻ (Fig. S2). No pronounced weight loss was found in the following calcination process, and the total weight loss fitted well with the theoretical composition of Cu_{1.1}Zn_{1.9}(BTC)₂·9.4(H₂O).

After calcination at 400 °C, Cu_xZn_{3-x}(BTC)₂·9.4(H₂O) transformed into a polycrystalline particles consisting of CuO and ZnO [49,50]. Fig. 4 showed the XRD patterns of Cu_xZn_{3-x}O₃ derived from Cu_xZn_{3-x}-HKUST-1. It can be found that primary structure of the framework collapsed and the characteristic diffraction peaks of HKUST-1 disappeared completely. CuO (JCPDS 00-045-0937) and ZnO (JCPDS 01-079-9878) were detected in all calcined samples. The calculated crystalline size of CuO in Cu_{2.8}Zn_{0.2}O₃, Cu_{1.7}Zn_{1.3}O₃ and Cu_{1.1}Zn_{1.9}O₃ was 22.1, 23.7 and 22.8 nm, respectively (Table S1). These crystals were clearly observed in their SEM images (Fig. S3), and their size distribution was summarized in Fig. S3B, in which 23–40 nm particles took up to 81.2% in frequency. The homogeneous dispersion of CuO and ZnO in the octahedron matrix of

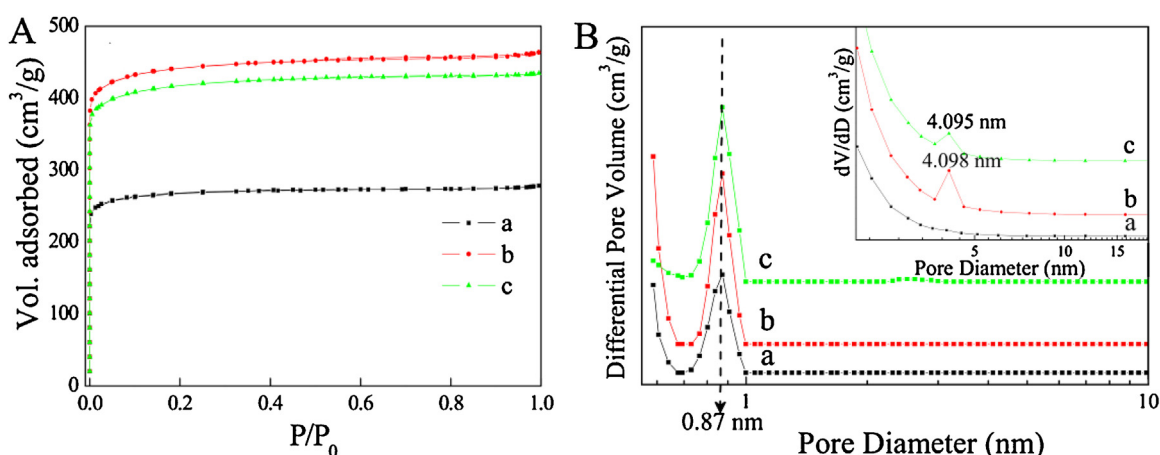


Fig. 2. N₂ adsorption isotherms (A) and pore volume distribution (B) of fresh Cu_{1.1}Zn_{1.9}-HKUST-1 (a), Cu_{1.7}Zn_{1.3}-HKUST-1 (b) and Cu_{2.8}Zn_{0.2}-HKUST-1 (c).

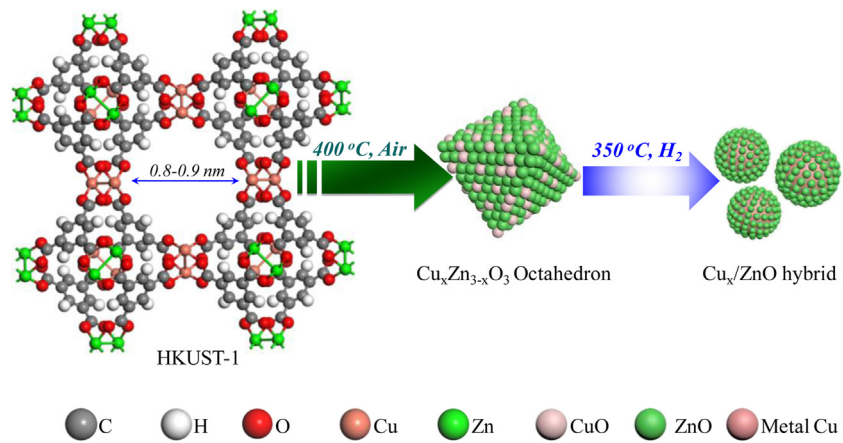


Fig. 3. Preparation of Cu/ZnO catalysts from Cu(Zn)-HKUST-1.

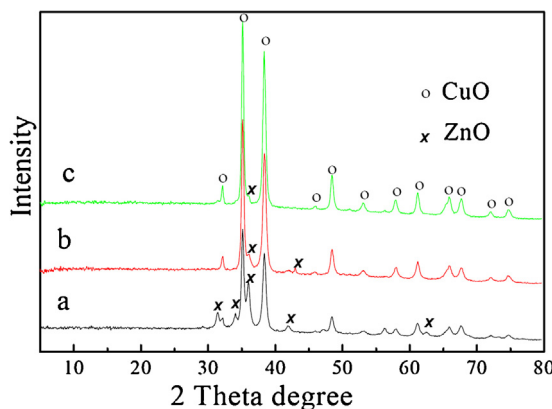


Fig. 4. XRD patterns of $\text{Cu}_{1.1}\text{Zn}_{1.9}\text{O}_3$ (a), $\text{Cu}_{1.7}\text{Zn}_{1.3}\text{O}_3$ (b), and $\text{Cu}_{2.8}\text{Zn}_{0.2}\text{O}_3$ (c).

$\text{Cu}_{1.1}\text{Zn}_{1.9}\text{O}_3$ was also confirmed in TEM images and its corresponding EDS mapping (Fig. S4).

Nitrogen adsorption–desorption isotherms of $\text{Cu}_{1.1}\text{Zn}_{1.9}\text{O}_3$, and the reference samples (Cu-ZnO-SF and Cu-ZnO-CP) were shown in Fig. S5. $\text{Cu}_{1.1}\text{Zn}_{1.9}\text{O}_3$ and Cu-ZnO-SF presented type II curve according to the IUPAC classification. These results inferred that mainly macro pores formed in these samples because of the aggregation of metal oxide particiles and plate-like layers [28]. The isotherms of Cu-ZnO-CP showed a H_4 -type hysteresis loop, indicating the existence of mesoporous channels. SEM analysis confirmed that

Cu-ZnO-SF was an aggregation of plate-like layers (Fig. S6A), and Cu-ZnO-CP appeared to be loose flocs containing smaller sized CuO and ZnO crystallites (Fig. S6B).

Fig. 5 presented the XPS spectra of Cu $2p_{3/2}$ and O 1s in $\text{Cu}_x\text{Zn}_{3-x}\text{O}_3$ derived from $\text{Cu}_x\text{Zn}_{3-x}$ -HKUST-1. The profiles of Cu $2p_{3/2}$ centered at 931.9, 932.0 and 932.2 eV in $\text{Cu}_{1.1}\text{Zn}_{1.9}\text{O}_3$, $\text{Cu}_{1.7}\text{Zn}_{1.3}\text{O}_3$ and $\text{Cu}_{2.8}\text{Zn}_{0.2}\text{O}_3$, respectively (Fig. 5A). This increased binding energy of Cu $2p_{3/2}$ could be attributed to the decreasing content of Zn. The spectra of O 1s could be deconvoluted into three peaks centered at 528.6, 530.5 and 531.5 eV (Fig. 5B), which was attributed to the oxygen in CuO [51], Cu-O-Zn [51,52] and ZnO [53] (Table S2). These results indicated that the interaction between CuO and ZnO was strengthened in $\text{Cu}_{1.1}\text{Zn}_{1.9}\text{O}_3$, which derived from calcined $\text{Cu}_{1.1}\text{Zn}_{1.9}$ -HKUST-1. XPS analysis of those reference samples (Cu-ZnO-SF and Cu-ZnO-CP) was presented in Fig. S7. The binding energy of Cu $2p_{3/2}$ in Cu-ZnO-SF (932.8 eV) and Cu-ZnO-CP (933.6 eV) was higher than that of $\text{Cu}_{1.1}\text{Zn}_{1.9}\text{O}_3$ (931.9 eV), which meant that the interaction between CuO and ZnO in reference catalysts was weaker. The deconvoluted peaks of O 1s (Fig. S7B, Table S2) also confirmed that the proportion of oxygen in the form of Cu-O-Zn in reference catalysts was less than that in $\text{Cu}_{1.1}\text{Zn}_{1.9}\text{O}_3$.

The reducibility of $\text{Cu}_x\text{Zn}_{3-x}\text{O}_3$ catalyst was displayed in Fig. S8. It was found that the initial reduction temperature, the center temperature of their reduction profiles and the total H_2 consumption increased gradually with the increasing content of Cu, and all Cu species could be reduced to Cu^0 below 315 °C. These results indicated that ZnO in the hybrid promoted the reduction of CuO

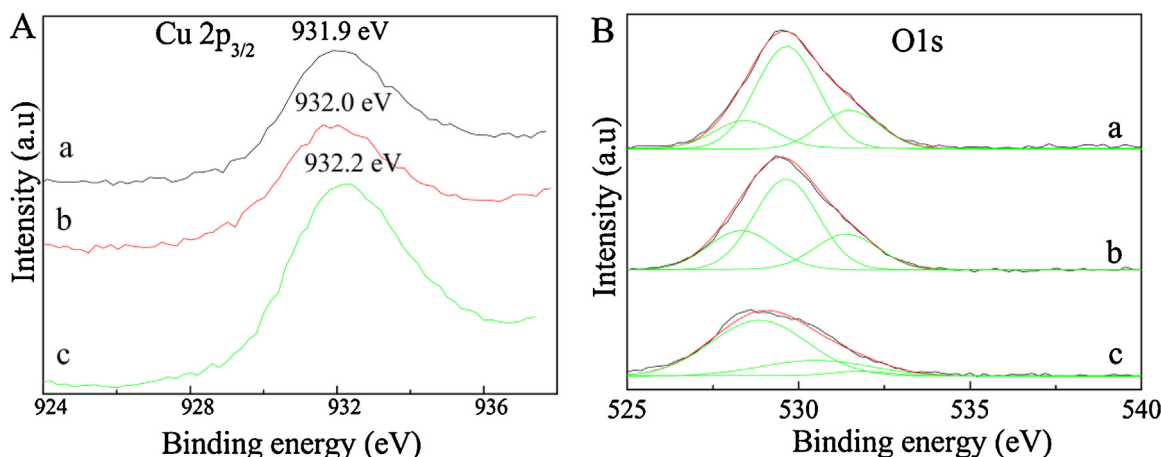


Fig. 5. XPS results of Cu $2p_{3/2}$ (A) and O 1s (B) in $\text{Cu}_{1.1}\text{Zn}_{1.9}\text{O}_3$ (a), $\text{Cu}_{1.7}\text{Zn}_{1.3}\text{O}_3$ (b), and $\text{Cu}_{2.8}\text{Zn}_{0.2}\text{O}_3$ (c).

[21,29]. H₂-TPR profiles of Cu-ZnO catalysts synthesized via different methods were displayed in Fig. S9. It was found that initial reduction temperature of Cu_{1.1}Zn_{1.9}O₃ was also lower than the reference catalysts. Fig. 6 showed in-situ XRD spectra of reduced Cu_{1.1}Zn_{1.9}O₃ at different temperature in 5% H₂/Ar flow. The intensity of the characteristic diffraction peaks of CuO (002) and (111) decreased gradually with increasing temperature and the reflection of Cu (111) appeared above 275 °C. CuO was reduced to Cu entirely above 300 °C.

3.3. The properties of reduced Cu_x/ZnO-catalysts

XPS spectra of Cu 2p_{3/2} in reduced catalysts were presented in Fig. S10 and the surface composition of Cu and Zn in these samples was summarized in Table 1. It was found that the binding energy of Cu 2p_{3/2} in Cu_{1.1}/ZnO located at 930.4 eV, but this value in Cu_{1.7}/ZnO and Cu_{2.8}/ZnO increased to 930.8 and 931.2 eV, respectively, which might be attributed to that partial amount of surface Cu atoms were oxidized before XPS measurement. At the same time, the detected mole ratio of Zn/Cu in Cu_{1.1}/ZnO, Cu_{1.7}/ZnO, Cu_{2.8}/ZnO and Cu/ZnO-SF increased obviously from 1.63, 0.75, 0.06 and 1.62 (in bulk and before reduction) to 3.07, 0.85, 0.10 and 3.84, respectively (see Table 1). These results indicated that ZnO located mainly on the surface of above reduced catalysts. But the mole ratio of Zn/Cu in reduced Cu/ZnO-CP exhibited an opposite tendency, which means that the structure of Cu/ZnO-CP would be different with above catalysts.

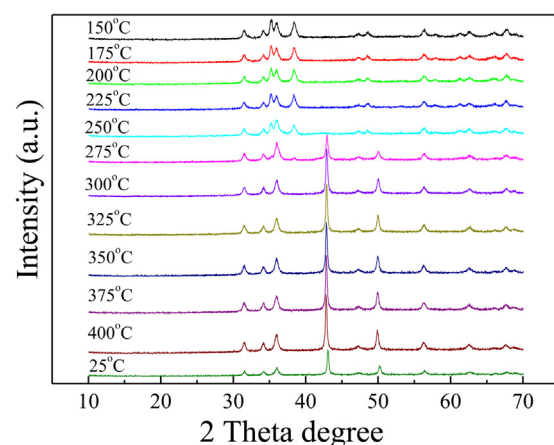


Fig. 6. In-situ XRD of reduced Cu_{1.1}Zn_{1.9}O₃ at different temperature in 5% H₂/Ar flow 25 °C: reduced catalysts cooled down to room temperature.

Fig. 7A revealed the high resolution TEM images of Cu_{1.1}/ZnO (the reduced state of Cu_{1.1}Zn_{1.9}O₃). The lattice fringes ascribed to Cu (blue square) and ZnO (green square) confirmed a core-shell ZnO@Cu framework, in which Cu particles were dotted with fine ZnO particles (the diagram of this structure was shown in Fig. 8A). Line-scan EDS analysis (Fig. 7A₃) further confirmed the proposed structure of Cu_{1.1}/ZnO (Fig. 8A). As a reference catalyst, Cu/ZnO-SF had a similar bulk composition as Cu_{1.1}/ZnO, but TEM analysis

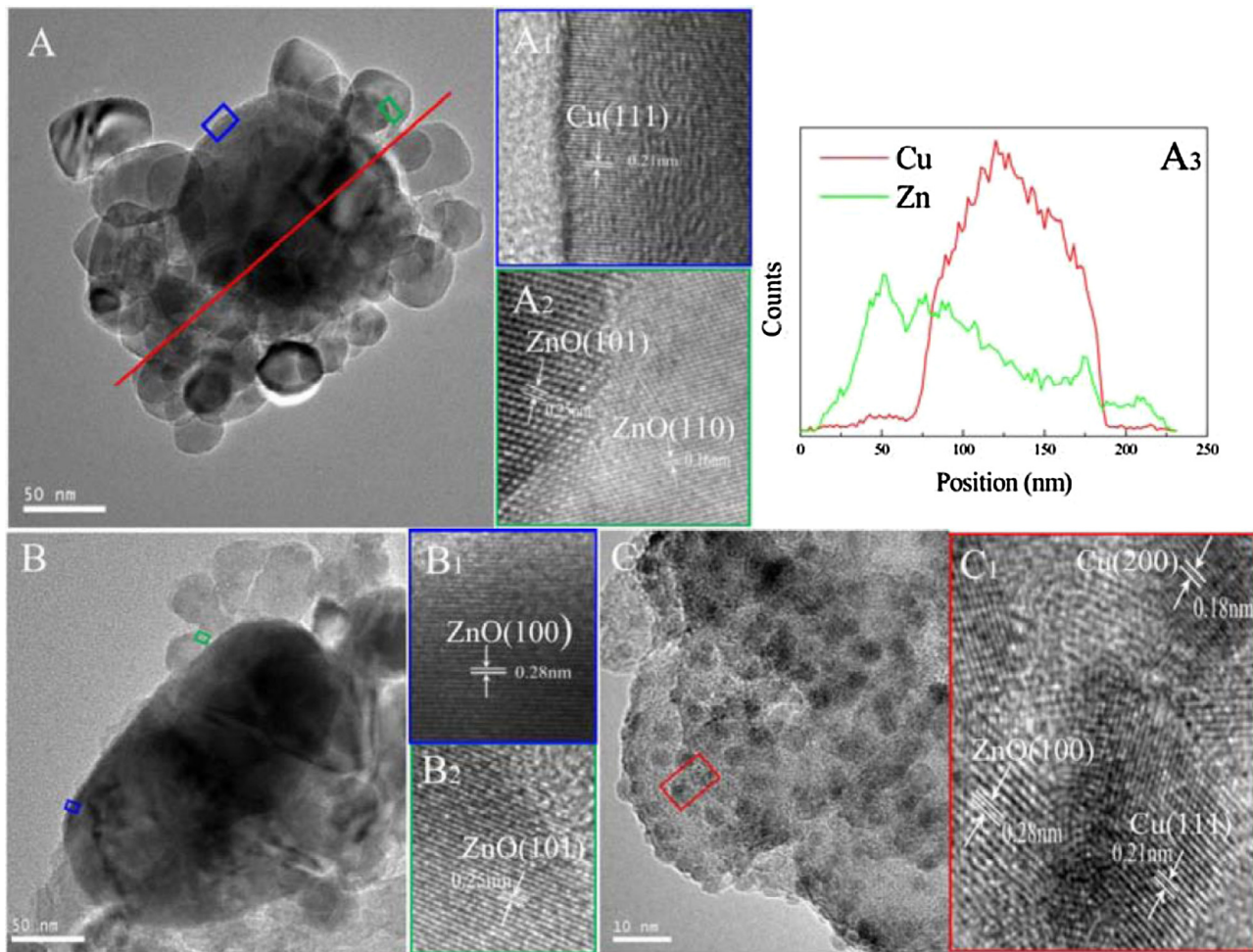


Fig. 7. TEM images of Cu_{1.1}/ZnO (A, A₁, A₂), Cu/ZnO-SF (B, B₁, B₂), Cu/ZnO-CP (C, C₁) and Line-EDS of Cu_{1.1}/ZnO (A₃).

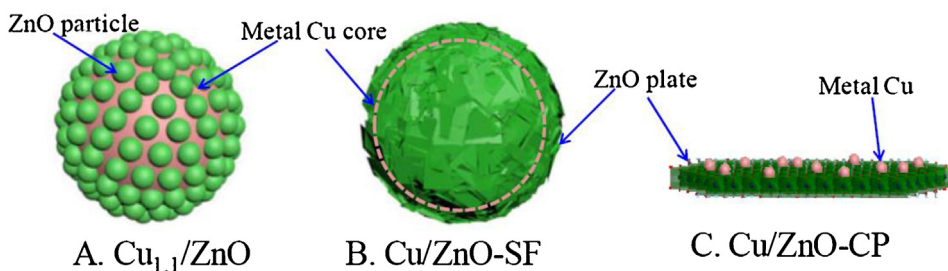


Fig. 8. Schematic diagram of prepared Cu-ZnO catalysts via different method.

confirmed that Cu particles were completely covered with plate-like ZnO (rather than ZnO particle in $\text{Cu}_{1.1}/\text{ZnO}$) in Cu/ZnO-SF (see Fig. 7B and the diagram in Fig. 8B). And the mole ratio of Zn/Cu in Cu/ZnO-SF also increased from 1.62 (in bulk) to 3.84 (on surface) (see Table 1). On the other hand, well dispersed Cu particles were observed clearly on the surface ZnO plate in reduced Cu/ZnO-CP. These images fitted well with above XPS analysis, and the proposed structure of these catalysts was shown in Fig. 8.

The active surface area and the dispersion of Cu in reduced Cu_x/ZnO catalysts were summarized in Table S1. It was found that the active surface area of Cu in reduced $\text{Cu}_{2.8}/\text{ZnO}$, $\text{Cu}_{1.7}/\text{ZnO}$ and $\text{Cu}_{1.1}/\text{ZnO}$ were 2.8, 12.1 and 31.9 ($\text{m}^2/\text{g-Cu}$), respectively. And the calculated particle size of Cu in these catalysts was 238.1, 55.9 and 21.1 nm, respectively. These results inferred that partially substitution of Cu with Zn in $\text{Cu}_x\text{Zn}_{3-x}(\text{BTC})_2\cdot 9.4(\text{H}_2\text{O})$ precursors increased the dispersion of Cu in Cu_x/ZnO catalysts. XRD analysis also confirmed that the particle size of Cu in the fresh reduced $\text{Cu}_{1.1}/\text{ZnO}$ was 23.7 nm (see Table S3).

3.4. Hydrogenolysis of glycerol

3.4.1. Performance of Cu/ZnO catalysts prepared via different methods

Fig. 9 compared the performance of Cu/ZnO catalysts prepared via different methods for the continuous hydrogenolysis of glycerol in a vertical fixed-bed reactor at 250 °C, 2.0 MPa. It was found that $\text{Cu}_{1.1}/\text{ZnO}$ exhibited a prominent activity and stability for this reaction. On $\text{Cu}_{1.1}/\text{ZnO}$, the detected conversion of glycerol reached 85.7% with a 82.3% selectivity of 1,2-PDO (at 2 h on stream), and the specific activity of surface Cu atom reached 100.4 mol-glycerol/mol-Cu/h. At the same time, it was interesting to note that the conversion of glycerol and the selectivity of 1,2-PDO remained stable during 17 h on stream. Besides 1,2-PDO, only acetol was detected as an intermediate [19].

As reference catalysts, the initial activity of $\text{Cu}/\text{ZnO-CP}$ was similar as that of $\text{Cu}_{1.1}/\text{ZnO}$, but it deactivated as the detected conversion of glycerol decreased continuously from 84.5% (at 2 h) to 45.1% (at 17 h), and the selectivity of 1,2-PDO also decreased from 89.2% to 77.6% after 17 h on stream. The calculated specific activity of surface Cu atom was 34.9 mol-glycerol/mol-Cu/h. The activity of $\text{Cu}/\text{ZnO-SF}$ was much lower, and it deactivated quickly in the first 5 h on stream.

These results indicated that the continuous hydrogenolysis of glycerol was a structure-sensitive process. As a reference, the composition of $\text{Cu}/\text{ZnO-SF}$ was similar as that of $\text{Cu}_{1.1}/\text{ZnO}$ (see Table 1), the active surface area and the dispersion of Cu in $\text{Cu}/\text{ZnO-SF}$ were slightly higher than that of $\text{Cu}_{1.1}/\text{ZnO}$ (see Table S1), but its activity was quite low (see Fig. 9). TEM (Fig. 7B) and XPS (see Table 1) analysis disclosed that most Cu particles were covered with plate-like ZnO in Cu/ZnO-SF (see Fig. 8B). In this case, these ZnO layers would block the accessibility of Cu to reactants and then depress its activity. On the contrary, Cu particles were only partially covered with nano sized ZnO in $\text{Cu}_{1.1}/\text{ZnO}$ (see Figs. 7 A and 8 A), this architecture

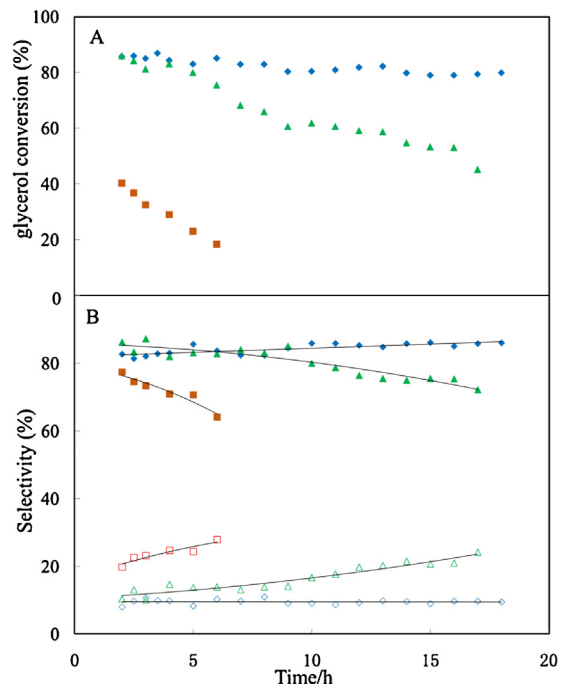


Fig. 9. Conversion of glycerol (A) and selectivity (B) of 1,2-PD (solid symbol) and acetol (hollow symbol) on $\text{Cu}_{1.1}/\text{ZnO}$ (rhombus), $\text{Cu}/\text{ZnO-SF}$ (square), and $\text{Cu}/\text{ZnO-CP}$ (triangle) in hydrogenolysis. Reaction conditions: catalyst, 0.10 g; 250 °C; 2.0 MPa, 20 wt% of glycerol aqueous solution 0.02 mL/min, and $\text{H}_2/\text{glycerol}=80$ (mol) in feed; data acquisition after steady operation for 2 h.

would enhance the adsorption and activation of H_2 (see Fig. S11) and accelerate the hydrogenolysis of glycerol.

Furthermore, these nano sized ZnO partially covered Cu particles (in $\text{Cu}_{1.1}/\text{ZnO}$) were more stable than ZnO plate supported Cu particles (in $\text{Cu}/\text{ZnO-CP}$). As another reference catalyst, the surface area and the dispersion of Cu in $\text{Cu}/\text{ZnO-CP}$ were obviously higher than that of $\text{Cu}_{1.1}/\text{ZnO}$ (see Table S1), but the stability of $\text{Cu}/\text{ZnO-CP}$ was poor compared with $\text{Cu}_{1.1}/\text{ZnO}$ (Fig. 9A). Characterization of the spent $\text{Cu}/\text{ZnO-CP}$ indicated that Cu particles sintered obviously from 6.0 (in fresh) to 23.7 nm (in spent $\text{Cu}/\text{ZnO-CP}$), while ZnO partially covered Cu particles (in $\text{Cu}_{1.1}/\text{ZnO}$) remained stable during 17 h on stream (see Table S3).

On the base of the structure and the performance of $\text{Cu}_{1.1}/\text{ZnO}$, $\text{Cu}/\text{ZnO-CP}$ and $\text{Cu}/\text{ZnO-SF}$ (see Fig. 8), we thought that the activity of these catalysts depended mainly on the interfacial area between Cu and ZnO, rather than on the particle size and/or dispersion of Cu. The outline and the microstructure of $\text{Cu}_{1.1}/\text{ZnO}$ and $\text{Cu}/\text{ZnO-CP}$ were quite different to each other, but they had similar initial activity, and both of them were more active than $\text{Cu}/\text{ZnO-SF}$. The higher initial activity of $\text{Cu}_{1.1}/\text{ZnO}$ and $\text{Cu}/\text{ZnO-CP}$ could be attributed to the fact that the interfacial area between Cu and ZnO was higher,

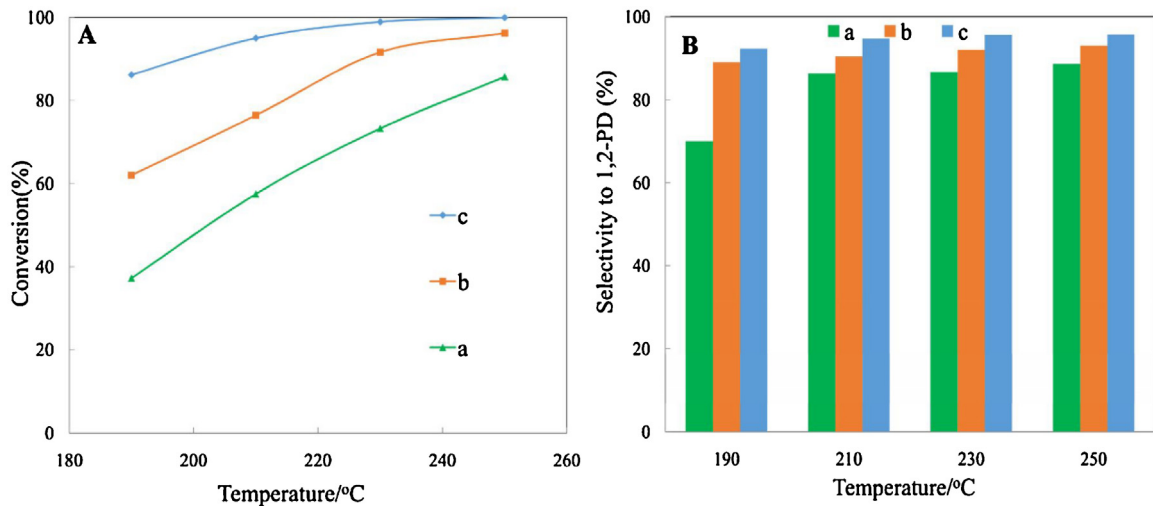


Fig. 10. (A) Conversion of glycerol and (B) Selectivity of 1,2-PD over $\text{Cu}_{1.1}/\text{ZnO}$ under different LHSV of 12 h^{-1} (a), 4.8 h^{-1} (b) and 2.4 h^{-1} (c). Reaction conditions: 2.0 MPa , 20 wt\% of glycerol aqueous solution, and $\text{H}_2/\text{glycerol} = 80$ (mol) in feed; data acquisition after steady operation for 2 h .

because ZnO particles on the surface of Cu could boost its activity [2]. H_2 -TPD experiments (Fig. S11) also confirmed that H_2 adsorbed strongly on $\text{Cu}_{1.1}/\text{ZnO}$, which would bring the formation of active $\text{H}-\text{H}$ and improve the activity for hydrogenolysis of glycerol [30]. The lower stability of Cu/ZnO -CP could be attributed to the phenomenon that Cu particles on ZnO plate sintered easily during the time on stream (see Table S3). On the other hand, nano sized ZnO partially covered Cu particles in $\text{Cu}_{1.1}/\text{ZnO}$ was stable because these ZnO particles functioned as a physical space between Cu particles and depressed the sintering of Cu .

3.4.2. Hydrogenolysis of glycerol over $\text{Cu}_{1.1}/\text{ZnO}$

Fig. 10 presented the performance of $\text{Cu}_{1.1}/\text{ZnO}$ for the hydrogenolysis of glycerol under different weight hourly space velocity (WHSV) and temperature. It was found that the conversion of glycerol and the selectivity of 1,2-PDO increased with the decreased WHSV and increasing temperature. Besides 1,2-PDO, acetol was detected as the only byproduct in these experiments. At higher WHSV (12 h^{-1}), the conversion of glycerol and the selectivity of 1,2-PDO increased continuously from 37.2% and 70.0% (at 190°C) to 85.7% and 82.3% (at 250°C), respectively. Under lower WHSV (2.4 h^{-1}), the conversion of glycerol reached to $>99\%$ at 230°C and the selectivity of 1,2-PDO was higher than 95.6%.

3.4.3. Performance Cu_x/ZnO catalysts synthesized from HKUST-1

The performance of Cu_x/ZnO catalysts that synthesized via different $\text{Cu}(\text{Zn})$ -HKUST-1 precursors were shown in Fig. 11, and the product distribution in these experiments were summarized in Table S4. It was confirmed that all these catalysts were efficient for the hydrogenolysis of glycerol, but the conversion of glycerol decreased with the increasing Cu/Zn mole ratio. This phenomenon also confirmed that the interfacial area between Cu and ZnO played a crucial role in the hydrogenolysis of glycerol [1].

4. Conclusion

In summary, we found that nano sized ZnO particles dotted on Cu hybrid ($\text{Cu}_{1.1}/\text{ZnO}$) could be synthesized via the controlled calcination and reduction of $\text{Cu}_{1.1}\text{Zn}_{1.9}(\text{BTC})_2 \cdot 9.4(\text{H}_2\text{O})$. TG-DSC and in situ XRD analysis indicated that $\text{Cu}_{1.1}\text{Zn}_{1.9}(\text{BTC})_2 \cdot 9.4(\text{H}_2\text{O})$ decomposed to octahedron structured $\text{Cu}_{1.1}\text{Zn}_{1.9}\text{O}_3$ above 350°C and $\text{Cu}_{1.1}\text{Zn}_{1.9}\text{O}_3$ could be reduced to $\text{Cu}_{1.1}/\text{ZnO}$ below 315°C . This novel structured $\text{Cu}_{1.1}/\text{ZnO}$ catalyst was extremely active and stable

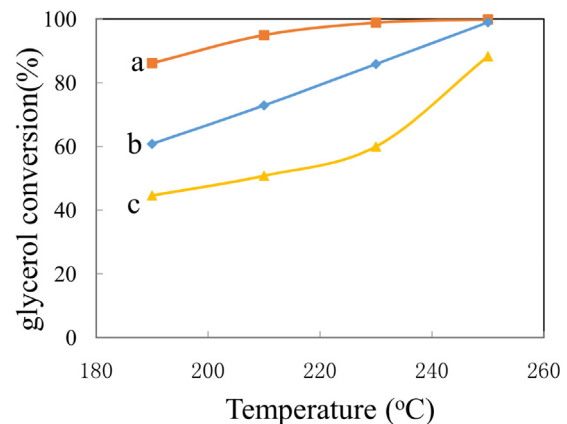


Fig. 11. Hydrogenolysis of glycerol at different temperature. $\text{Cu}_{1.1}/\text{ZnO}$ (a), $\text{Cu}_{1.7}/\text{ZnO}$ (b), and $\text{Cu}_{2.8}/\text{ZnO}$ (c). Reaction conditions: catalyst, 0.50 g ; 2.0 MPa , 20 wt\% of glycerol aqueous solution $0.02 \text{ mL}/\text{min}$, and $\text{H}_2/\text{glycerol} = 80$ (mol) in feed; data acquisition after steady operation for 2 h .

for the continuous hydrogenolysis of glycerol in a fixed-bed reactor. The specific activity of surface Cu atom in $\text{Cu}_{1.1}/\text{ZnO}$ reached $100.4 \text{ mol-glycerol/mol-Cu/h}$ (at 250°C). Characterization results confirmed that hydrogenolysis of glycerol in continuous fixed-bed reactor was a structure-sensitive process, and the activity of Cu/ZnO catalysts depended strongly on the interfacial area between Cu and ZnO .

Acknowledgments

This research work was supported by the National Natural Science Foundation of China (Contract No. 21473155, 21273198), Zhejiang Provincial Natural Science Foundation (Grant No. LZ12B03001).

Appendix A. Supplementary data

Supplementary data associated with this article can be found, in the online version, at <http://dx.doi.org/10.1016/j.apcatb.2016.10.011>.

References

[1] M. Behrens, F. Studt, I. Kasatkin, S. Kühl, M. Hävecker, F. Abild-Pedersen, S. Zander, F. Girsdsies, P. Kurr, B.-L. Kniep, M. Tovar, R.W. Fischer, J.K. Nørskov, R. Schlögl, *Science* 336 (2012) 893–897.

[2] S. Kuld, M. Thorhauge, H. Falsig, C.F. Elkjaer, S. Helveg, I. Chorkendorff, J. Sehested, *Science* 352 (2016) 969–974.

[3] S.A. Kondrat, P.J. Smith, P.P. Wells, P.A. Chater, J.H. Carter, D.J. Morgan, E.M. Fiordaliso, J.B. Wagner, T.E. Davies, L. Lu, J.K. Bartley, S.H. Taylor, M.S. Spencer, C.J. Kiely, G.J. Kelly, C.W. Park, M.J. Rosseinsky, G.J. Hutchings, *Nature* 531 (2016) 83–87.

[4] M. Iwamoto, H. Hamada, *Catal. Today* 10 (1991) 57–71.

[5] M. Turco, G. Bagnasco, U. Costantino, F. Marmottini, T. Montanari, G. Ramis, G. Busca, *J. Catal.* 228 (2004) 43–55.

[6] A. Kubacka, M. Fernández-García, A. Martínez-Arias, *Appl. Catal. A* 518 (2016) 2–17.

[7] C.-H. Zhou, J.N. Beltramini, Y.-X. Fan, G.Q. Lu, *Chem. Soc. Rev.* 37 (2008) 527–549.

[8] B. Lorenzut, T. Montini, L. De Rogatis, P. Canton, A. Benedetti, P. Fornasiero, *Appl. Catal. B* 101 (2011) 397–408.

[9] S.D. Jones, L.M. Neal, H.E. Hagelin-Weaver, *Appl. Catal. B* 84 (2008) 631–642.

[10] C.P. Jiménez-Gómez, J.A. Cecilia, D. Durán-Martín, R. Moreno-Tost, J. Santamaría-González, J. Mérida-Robles, R. Mariscal, P. Maireles-Torres, *J. Catal.* 336 (2016) 107–115.

[11] J. Cui, J. Tan, X. Cui, Y. Zhu, T. Deng, G. Ding, Y. Li, *ChemSusChem* 9 (2016) 1259–1262.

[12] S. Wang, H. Liu, *Catal. Lett.* 117 (2007) 62–67.

[13] J. Chaminand, L.A. Djakovitch, P. Gallezot, P. Marion, C. Pinel, C. Rosier, *Green Chem.* 6 (2004) 359–361.

[14] E.S. Vasiliadou, V.L. Yfanti, A.A. Lemonidou, *Appl. Catal. B* 163 (2015) 258–266.

[15] H. Tan, M.N. Hedhill, Y. Wang, J. Zhang, K. Li, S. Sioud, Z.A. Al-Talla, M.H. Amad, T. Zhan, O.E. Tall, Y. Han, *Catal. Sci. Technol.* 3 (2013) 3360–3370.

[16] C. Wang, H. Jiang, C. Chen, R. Chen, W. Xing, *Chem. Eng. J.* 264 (2015) 344–350.

[17] Y. Du, C. Wang, H. Jiang, C. Chen, R. Chen, *J. Ind. Eng. Chem.* 35 (2016) 262–267.

[18] Y. Feng, H. Yin, A. Wang, L. Shen, L. Yu, T. Jiang, *Chem. Eng. J.* 168 (2011) 403–412.

[19] A. Bienholz, H. Hofmann, P. Claus, *Appl. Catal. A* 391 (2011) 153–157.

[20] D. Sun, Y. Yamada, S. Sato, W. Ueda, *Appl. Catal. B* 193 (2016) 75–92.

[21] F. Cai, W. Zhu, G. Xiao, *Catal. Sci. Technol.* 6 (2016) 4889–4900.

[22] C. Liu, C. Zhang, S. Hao, S. Sun, K. Liu, J. Xu, Y. Zhu, Y. Li, *Catal. Today* 261 (2016) 116–127.

[23] Y. Nakagawa, K. Tomishige, *Catal. Sci. Technol.* 1 (2011) 179–190.

[24] Y. Wang, J. Zhou, X. Guo, *RSC Adv.* 5 (2015) 74611–74628.

[25] G. Yang, N. Tsubaki, J. Shamoto, Y. Yoneyama, Y. Zhang, *J. Am. Chem. Soc.* 132 (2010) 8129–8136.

[26] E.S. Vasiliadou, T.M. Eggenhuisen, P. Munnik, P.E. de Jongh, K.P. de Jong, A.A. Lemonidou, *Appl. Catal. B* 145 (2014) 108–119.

[27] R. van den Berg, J. Zečević, J. Sehested, S. Helveg, P.E. de Jongh, K.P. de Jong, *Catal. Today* 272 (2016) 87–93.

[28] Z. Yuan, L. Wang, J. Wang, S. Xia, P. Chen, Z. Hou, X. Zheng, *Appl. Catal. B* 101 (2011) 431–440.

[29] S. Zhu, X. Gao, Y. Zhu, W. Fan, J. Wang, Y. Li, *Catal. Sci. Technol.* 5 (2015) 1169–1180.

[30] S. Xia, R. Nie, X. Lu, L. Wang, P. Chen, Z. Hou, *J. Catal.* 296 (2012) 1–11.

[31] Z. Yuan, J. Wang, L. Wang, W. Xie, P. Chen, Z. Hou, X. Zheng, *Biol. Technol.* 101 (2010) 7088–7092.

[32] M. Behrens, A. Furche, I. Kasatkin, A. Trunschke, W. Busser, M. Muhler, B. Kniep, R. Fischer, R. Schlögl, *ChemCatChem* 2 (2010) 816–818.

[33] S. Kuld, C. Conradsen, P.G. Moses, I. Chorkendorff, J. Sehested, *Angew. Chem. Int. Ed.* 53 (2014) 5941–5945.

[34] S.L. James, *Chem. Soc. Rev.* 32 (2003) 276–288.

[35] H. Furukawa, K.E. Cordova, M. O'Keeffe, O.M. Yaghi, *Science* 341 (2013) 1230444. 1–1230444.12.

[36] R. Wu, X. Qian, F. Yu, H. Liu, K. Zhou, J. Wei, Y. Huang, *J. Mater. Chem. A* 1 (2013) 11126–11129.

[37] J.-D. Xiao, Q. Shang, Y. Xiong, Q. Zhang, Y. Luo, S.-H. Yu, H.-L. Jiang, *Angew. Chem. Int. Ed.* 55 (2016) 1–6.

[38] L. Pan, T. Muhammad, L. Ma, Z.-F. Huang, S. Wang, L. Wang, J.-J. Zou, X. Zhang, *Appl. Catal. B* 189 (2016) 181–191.

[39] W. Du, G. Chen, R. Nie, Y. Li, Z. Hou, *Catal. Commun.* 41 (2013) 56–59.

[40] D.F. Sava Gallis, M.V. Parkes, J.A. Greathouse, X. Zhang, T.M. Nenoff, *Chem. Mater.* 27 (2015) 2018–2025.

[41] B. An, K. Cheng, C. Wang, Y. Wang, W. Lin, *ACS Catal.* 6 (2016) 3610–3618.

[42] S.S.-Y. Chui, S.M.-F. Lo, J.P.H. Charmant, A.G. Orpen, I.D. Williams, *Science* 283 (1999) 1148–1150.

[43] H. Liu, L. Chang, C. Bai, L. Chen, R. Luque, Y. Li, *Angew. Chem. Int. Ed.* 55 (2016) 5019–5023.

[44] J. Zhao, W.T. Nunn, P.C. Lemaire, Y. Lin, M.D. Dickey, C.J. Oldham, H.J. Walls, G.W. Peterson, M.D. Losego, G.N. Parsons, *J. Am. Chem. Soc.* 137 (2015) 13756–13759.

[45] W. Du, L. Zheng, X. Li, J. Fu, X. Lu, Z. Hou, *Appl. Clay Sci.* 123 (2016) 166–172.

[46] C.J.G. Van Der Grift, A.F.H. Wielaars, B.P.J. Jogh, J. Van Beunum, M. De Boer, M. Versluijs-Helder, J.W. Geus, *J. Catal.* 131 (1991) 178–189.

[47] J.I. Feldblyum, M. Liu, D.W. Gidley, A.J. Matzger, *J. Am. Chem. Soc.* 133 (2011) 18257–18263.

[48] M.K. Bhunia, J.T. Hughes, J.C. Fettinger, A. Navrotsky, *Langmuir* 29 (2013) 8140–8145.

[49] C. Holse, C.F. Elkjaer, A. Nierhoff, J. Sehested, I. Chorkendorff, S. Helveg, J.H. Nielsen, *J. Phys. Chem. C* 119 (2015) 2804–2812.

[50] S. Zhang, H. Liu, P. Liu, Z. Yang, X. Feng, F. Huo, X. Lu, *Nanoscale* 7 (2015) 9411–9415.

[51] J.A. Anderson, J.L.G. Fierro, *J. Solid State Chem.* 108 (1994) 305–313.

[52] S. Xia, L. Zheng, L. Wang, P. Chen, Z. Hou, *RSC Adv.* 3 (2013) 16569–16576.

[53] E.C. Onyiriuka, *J. Non Cryst. Solids* 163 (1993) 268–273.